Monthly Notices
of the
ROYAL ASTRONOMICAL SOCIETY

Mon. Not. R. Astron. Soc. **410,** 2123–2136 (2011) doi:10.1111/j.1365-2966.2010.17585.x

Gravitational wave background from sub-luminous GRBs: prospects for second- and third-generation detectors

E. Howell,[1⋆] T. Regimbau,[2] A. Corsi,[3] D. Coward[1] and R. Burman[1]

[1] *School of Physics, University of Western Australia, Crawley WA 6009, Australia*
[2] *UMR ARTEMIS, CNRS, University of Nice Sophia-Antipolis, Observatoire de la Côte d'Azur, BP 4229, 06304 Nice, Cedex 4, France*
[3] *18-34 LIGO Laboratory, California Institute of Technology, Pasadena, CA 91125, USA*

Accepted 2010 August 23. Received 2010 August 13

ABSTRACT

We assess the detection prospects of a gravitational wave background associated with sub-luminous gamma-ray bursts (SL-GRBs). We assume that the central engines of a significant proportion of these bursts are provided by newly born magnetars and consider two plausible GW emission mechanisms. First, the deformation-induced triaxial GW emission from a newly born magnetar. Secondly, the onset of a secular bar-mode instability, associated with the long-lived plateau observed in the X-ray afterglows of many gamma-ray bursts. With regards to detectability, we find that the onset of a secular instability is the most optimistic scenario: under the hypothesis that SL-GRBs associated with secularly unstable magnetars occur at a rate of (48–80) $\mathrm{Gpc^{-3}\ yr^{-1}}$ or greater, cross-correlation of data from two Einstein Telescopes (ETs) could detect the GW background associated to this signal with a signal-to-noise ratio of 3 or greater after 1 year of observation. Assuming neutron star spindown results purely from triaxial GW emissions, we find that rates of around (130–350) $\mathrm{Gpc^{-3}\ yr^{-1}}$ will be required by ET to detect the resulting GW background. We show that a background signal from secular instabilities could potentially mask a primordial GW background signal in the frequency range where ET is most sensitive. Finally, we show how accounting for cosmic metallicity evolution can increase the predicted signal-to-noise ratio for background signals associated with SL-GRBs.

Key words: gravitational waves – supernovae: general – cosmology: miscellaneous – gamma-ray bursts.

1 INTRODUCTION

The two closest recorded gamma-ray bursts (GRBs), GRB 980425 (36 Mpc) and GRB 060218 (145 Mpc), along with GRB 031203, associated with a host galaxy at ∼480 Mpc (Feng & Fox 2010), make up a sub-class of long-duration GRBs[1] (LGRBs) known as sub-luminous GRBs (SL-GRBs) (Cobb et al. 2006; Liang et al. 2007a; Guetta & Della Valle 2007; Virgili, Liang & Zhang 2009). This class of GRB has isotropic equivalent γ-ray energy emissions typically several orders of magnitude below those of standard long-duration GRBs (Murase et al. 2006; Guetta & Della Valle 2007; Imerito et al. 2008) suggesting that they could form a unique population of bursts.

Observations have confirmed that at least some LGRBs are associated with the deaths of massive stars (Woosley & Bloom 2006). One scenario for the generation of LGRBs is described by the collapsar model (Woosley 1993; MacFadyen, Woosley & Heger 2001). In this model, the inner part of a progenitor star [a Wolf–Rayet (WR) star] collapses, via a Type Ib/c supernova, forming a rapidly rotating black hole. High angular momentum enables the infalling matter to form an accretion disc, which in turn powers an ultra-relativistic jet (a 'fireball') that blasts through the stellar envelope (Mészáros & Rees 1992; Woosley 1993; Sari, Narayan & Piran 1998). A number of authors have suggested that, at least in some cases, GRB explosions may end in the formation of a highly magnetized neutron star (NS), i.e. a magnetar rather than a black hole (Usov 1992; Duncan & Thompson 1992; Dai & Lu 1998; Nakar 2007; Bucciantini et al. 2009; Zhang & Dai 2009). Additional support for this scenario has come from detailed modelling of the spectra and light curve of SN 2006aj (Type Ic), associated with GRB 060218. This analysis suggested that the explosion energy and ejected mass originated from a progenitor star with a zero-age main sequence mass of $\sim 20\ \mathrm{M_\odot}$, implying the birth of a NS rather than a black hole (Mazzali et al. 2006; Soderberg et al. 2006a). The fact that this burst was of the SL-GRB class suggests that a proportion of such bursts may well be powered by magnetars (Murase et al. 2006; Toma et al. 2007).

⋆E-mail: ejhowell@physics.uwa.edu.au

[1] Hereafter, we refer to long GRBs as those having a T_{90} duration >2 s in agreement with the traditional classification by Kouveliotou et al. (1993).

The magnetar scenario for GRBs has been invoked to explain recent observations by the *Swift* satellite,[2] showing that a significant fraction of the X-ray afterglows of GRBs exhibit a shallow decay phase lasting 10^2–10^4 s (Zhang et al. 2006; Fan & Xu 2006; Nousek et al. 2006; Liang, Zhang & Zhang 2007b; Yu, Liu & Dai 2007; Yamazaki 2009). A number of studies have suggested that the long-duration afterglow plateau may be powered by a newly born millisecond magnetar. This could channel slowly decreasing rotational energy into a relativistic outflow via magnetic dipole emission (Usov 1992; Zhang & Mèszàros 2001; Fan & Xu 2006; DallOsso et al. 2010; Lyons et al. 2010; Yu, Cheng & Cao 2010).

From the perspective of GW detection, the relative local proximity of observed SL-GRBs makes these sources appealing, and raises the possibility of multi-messenger observations by second- and third-generation GW detectors (Kochanek & Piran 1993; Kobayashi & Mészáros 2003; Abbott et al. 2008; Andersson et al. 2009; Bloom et al. 2009; Corsi & Mészáros 2009a,b; Abbott et al. 2010a,b). Any detection scenario, of course, depends on the frequency of events in the nearby Universe. Radio observations of 68 local SNe Ib/c by Soderberg et al. (2006b) show that less than 10 per cent were associated with LGRBs. Based on the local rate of Type Ib/c supernovae (Soderberg et al. 2006a; Guetta & Della Valle 2007) this yields an extreme upper limit of $\sim 2 \times 10^3\,\mathrm{Gpc^{-3}\,yr^{-1}}$ for SL-GRBs. Studies of SL-GRB rates over the last four years (to be discussed in the next section) have yielded estimates extending over a range (40–1800) $\mathrm{Gpc^{-3}\,yr^{-1}}$. These estimates are orders of magnitude greater than those of classical LGRBs.

Although these rate estimates are encouraging, GW detections will also depend on the strength of the emissions. As LGRBs require rapid rotation to produce an accretion disc, it is logical to consider post-collapse GW emission mechanisms equally dependent on rotation.

A first possibility is that the strong magnetic fields of newly born magnetars, of the order of 10^{14}–10^{16} G (Duncan & Thompson 1992), could lead to deformations that would dominate any flattening due to a fast rotation (Ostriker & Gunn 1969; Palomba 2000; Konno, Obata & Kojima 2000). If the deformation axis is offset from the spin axis, this could lead to GW emissions (Palomba 2001; Cutler 2002; Stella et al. 2005; Regimbau & de Freitas Pacheco 2006a; DallOsso & Stella 2007; DallOsso et al. 2009).

A second emission possibility, suggested by Corsi & Mészáros (2009a,b), is that GW emissions could accompany the electromagnetic dipole emissions of a newly formed magnetar via a secular bar-mode instability (Chandrasekhar 1970; Friedman & Schutz 1978; Lai & Shapiro 1995; Ou, Tohline & Lindblom 2004; Shibata & Karino 2004). As this instability occurs on a long time-scale, $\sim 10^2$–10^4 s, it corresponds well with the observed X-ray plateau of some LGRBs. We note that we do not consider the GW emissions from R modes (Owen et al. 1998; Ferrari, Matarrese & Schneider 1999b), as the effect of the magnetic field could suppress this GW instability in magnetars (Rezzolla et al. 2001; Mendell 2001).

Despite the observed sample of SL-GRBs being small, and the origin of this class of bursts still some way from being clearly understood, the rate estimates based on current observations are of an equivalent order to those of other sources of potentially detectable GW backgrounds, e.g. NS/NS mergers (Regimbau & de Freitas Pacheco 2006b; Regimbau 2007; Regimbau & Mandic 2008). For this reason, we are motivated in this paper to determine if a GW background from SL-GRBs, based on the two mechanisms outlined above, could produce a detectable signal for advanced GW interferometric detectors such as ALIGO[3] (Advanced Laser Interferometer Gravitational-wave Observatory) and VIRGO[4] or third-generation instruments such as the Einstein Telescope[5] (ET). Although we expect there to be variation in the single-source emission mechanisms, we take these models to represent average values. This assumption is reasonable, based on the fact that detection of a stochastic GW background can only yield information on the mean event emission of a population (Regimbau & Mandic 2008). Additionally, we allow for uncertainties in both the event rates of SL-GRBs and in the frequency of occurrence of the two GW emission mechanisms considered by employing widely separated upper and lower limits.

The possibility of a detectable continuous astrophysical background signal is important, as it could mask the relic GW background signal from the earliest epochs of the Universe. Primordial backgrounds are expected to be produced by large numbers of dynamical events in the early Universe (Grishchuk 1975) – this signal is expected to be isotropic, stationary and unpolarized. An upper limit on the energy density of the primordial GW background normalized by the critical energy density of the universe was recently set as $<6.9 \times 10^{-6}$ in the frequency band (41.5–169.25) Hz by the LIGO Scientific Collaboration and Virgo Collaboration using data from the S5 two-year science run (LSC VIRGO Collaboration 2009). This limit improved on previous indirect limits from the big bang nucleosynthesis and cosmic microwave background at around 100 Hz. As ET will be able to detect GW background signals around six orders of magnitude below this limit, it is possible that astrophysical GW background (AGB) signals could form an additional 'noise' component concealing the background signal from primordial processes.

The organization of the paper is as follows. In Section 2, we discuss the rate estimates of SL-GRBs and in Sections 3 and 4, we describe in more detail the two previously mentioned GW emission mechanisms that could result from newly formed magnetars in SL-GRBs. In Section 5, we describe how we will calculate a GW background spectrum and in Section 6 we discuss issues relevant to detection. In Sections 7 and 8, we present our estimations of the GW background signal from our two single-source emission mechanisms and finally draw our conclusions in Section 9.

2 RATE ESTIMATES OF SUB-LUMINOUS GRBS

Table 1 shows rate estimates of SL-GRBs from studies spanning the past four years. Estimates are generally determined by statistical arguments, or fits to the $\log N - \log P$, peak flux or 'brightness distribution' of bursts. Statistical arguments are typically based on the two closest sub-luminous bursts: GRB 980425 and GRB 060218, detected within two years of operation by *Swift*. As rates based on Poisson statistics could be affected by small number statistics, some authors choose to fit to the $\log N - \log P$ distribution of observed bursts. Using this method, a SL-GRB population can be accounted for by decreasing the lower bound of the luminosity function (LF) or by employing a two-component LF (Coward 2005).

The table shows that estimates extend over a range (40–1800) $\mathrm{Gpc^{-3}\,yr^{-1}}$, reflecting the present uncertainties on the nature of these bursts. For example, other than uncertainties in the LF, it is

[2] http://heasarc.gsfc.nasa.gov/docs/swift/swiftsc.html

[3] LIGO – http://www.ligo.caltech.edu/

[4] VIRGO – http://www.virgo.infn.it/

[5] ET – http://www.et-gw.eu/.

Table 1. A sample of the published estimates on the rate of SL-GRBs along with a brief description of how the rate was determined.

Reference	Rate estimate $\mathrm{Gpc^{-3}\,yr^{-1}}$	Notes
Soderberg et al. (2006a)	230^{+490}_{-190}	A Poisson statistical estimate based on the detection volumes for bursts similar to GRB 980425 and XRF 060218.
Pian et al. (2006)	110^{+180}_{-20}	A fit to the $\log N - \log P$ distribution of BATSE[a] data using a smoothed broken power-law LF with a lower bound set by GRB 980425.
Guetta & Della Valle (2007)	380^{+620}_{-225}[b] 200–1800[c] 110–1200[d]	Poisson statistical estimate determined as well as two fits to the $\log N - \log P$ distributions of both *Swift* and BATSE. A single power-law LF was used with a lower bound based on GRB 980425.
Liang et al. (2007a)	325^{+352}_{-177}	The LF and rate density are estimated using *Swift* bursts with known z.
Chapman et al. (2007)	700^{+360}_{-360}	Estimates obtained by correlating galaxies within 155 Mpc to BATSE bursts with properties similar to known SL-GRBs.
Virgilii et al. (2008)	200^{+200}_{-100}	LF parameters and z values estimated through simulation. Rate estimates obtained through statistical comparison with the observed *Swift* luminosity–z distribution.

[a]BATSE – the Burst and Transient Source Experiment on the Compton Gamma-Ray Observatory, launched in 1991, recorded 2704 GRBs during its 9 years of operation.
[b]Estimate based on Poisson statistics.
[c]Estimate based on BATSE data.
[d]Estimate based on *Swift* data.

Table 2. The sub-luminous GRB rate estimates used in this study. The estimates are denoted by upper, r_{U}, plausible, r_{P}, and lower, r_{L}.

	Rate estimate in $\mathrm{Gpc^{-3}\,yr^{-1}}$
r_{U}	1800
r_{P}	200
r_{L}	40

still not clear if these bursts are LGRBs viewed off-axially or are an intrinsically different population (see discussion in Coward 2005). Assuming that SL-GRBs are a unique population with an intrinsic difference in central engine from LGRBs, the rates we will adopt in this study are shown in Table 2.

For a plausible rate, we take the most recent estimate of Virgilii, Liang & Zhang (2008), $r_{\mathrm{P}} = 200\,\mathrm{Gpc^{-3}\,yr^{-1}}$. As shown in Table 2, this estimate is of a similar order to the most likely values published in the other studies. As an upper limit we take the largest estimate shown in Table 2 of $r_{\mathrm{U}} = 1800\,\mathrm{Gpc^{-3}\,yr^{-1}}$ (Guetta & Della Valle 2007) – this value is ∼9 per cent of the local rate of SNe Ib/c. We note that this is a similar fraction of SNe Ib/c producing magnetars to that of Type II SNe – around 10 per cent – as suggested by Murase et al. (2006) and Soderberg et al. (2006a). For our lower bound we take a value of $r_{\mathrm{L}} = 40\,\mathrm{Gpc^{-3}\,yr^{-1}}$. We obtain this value by taking a typical lower bound of around $100\,\mathrm{Gpc^{-3}\,yr^{-1}}$ based on the estimates shown in Table 2, and in correspondence with LGRBs observed during the *Swift* Era, we assume that 40 per cent of SL-GRBs will also have X-ray plateaus (Evans et al. 2009).

3 TRIAXIAL GW EMISSION FROM MAGNETARS

Rotating NSs with a triaxial shape have a time varying quadrupole moment and hence radiate GWs at a frequency, f, which is twice the rotational frequency. A NS born with a rotational period P_0 loses rotational energy through magnetic dipole torques and GW emission:

$$\frac{\mathrm{d}E_{\mathrm{rot}}}{\mathrm{d}t} = \frac{\mathrm{d}E_{\mathrm{dip}}}{\mathrm{d}t} + \frac{\mathrm{d}E_{\mathrm{gw}}}{\mathrm{d}t}\,, \tag{1}$$

with rotational, dipole and gravitational energy loss rates:

$$\begin{cases} \dfrac{\mathrm{d}E_{\mathrm{rot}}}{\mathrm{d}t} = \pi^2 I_{zz} f \dfrac{\mathrm{d}f}{\mathrm{d}t}, \\ \dfrac{\mathrm{d}E_{\mathrm{dip}}}{\mathrm{d}t} = K_{\mathrm{dip}} f^4 = \dfrac{\pi^4 R^6 B^2}{6c^3} f^4, \\ \dfrac{\mathrm{d}E_{\mathrm{gw}}}{\mathrm{d}t} = K_{\mathrm{gw}} f^6 = \dfrac{32\pi^6 G I_{zz}^2 \rho^2}{5c^5} f^6. \end{cases} \tag{2}$$

These result in a change in the frequency:

$$\frac{\mathrm{d}f}{\mathrm{d}t} = \frac{K_{\mathrm{dip}}}{\pi^2 I_{zz}} f^3 + \frac{K_{\mathrm{gw}}}{\pi^2 I_{zz}} f^5 \tag{3}$$

From the equations for $\mathrm{d}E_{\mathrm{gw}}/\mathrm{d}f$ and $\mathrm{d}f/\mathrm{d}t$, we can write the emitted GW spectral energy density as follows:

$$\frac{\mathrm{d}E_{\mathrm{gw}}}{\mathrm{d}f} = K f^3 \left(1 + \frac{K}{\pi^2 I_{zz}} f^2\right)^{-1} \quad \text{with} \quad f \in [0, 2/P_0] \tag{4}$$

where

$$K = \frac{192\pi^4 G I_{zz}^3}{5c^2 R^6} \frac{\rho^2}{B^2}\,. \tag{5}$$

In this expression R is the radius of the star, $\rho = (I_{xx} - I_{yy})/I_{zz}$ is the ellipticity in terms of the principal moments of inertia, $B = B_{\mathrm{s}} \sin\alpha$ where B_{s} is the surface polar magnetic field strength and α the angle between the rotational and dipole axes.

The majority of NSs are understood to be born with magnetic fields of the order of 10^{12}–10^{13} G and rotational periods of the order of tens or hundreds of milliseconds (Regimbau & de Freitas Pacheco 2000; Faucher-Giguère & Kaspi 2006; Soria et al. 2008) and will make a negligible contribution. However, NSs with sufficiently high initial rotational periods, ∼1–3 ms, which undergo violent convection or differential rotation during the first seconds after birth, can obtain super-strong crustal magnetic fields (B_{s} in the range $\sim 10^{14}$–10^{16} G) through an $\alpha - \Omega$ dynamo action (Duncan & Thompson 1992; Thompson & Duncan 1993). For these highly magnetized NSs, the distortion induced by the magnetic torque can

become significant (Palomba 2000; Konno et al. 2000), and GW emission can be orders of magnitudes larger than for ordinary NSs (Palomba 2001). Because it could carry away most of the initial rotational energy of millisecond magnetars, this scenario provides a natural explanation for the absence of the signature of enhanced energy injections in X-ray spectra of supernova remnants around known magnetars (DallOsso et al. 2009).

In this study, we take $P_0 = 1$ ms, and corresponding to a typical NS of mass 1.4 $M_\odot$ take $R = 10$ km and $I_{zz} = 1 \times 10^{38}$ kg m^2 (Arnett & Bowers 1976; Bonazzola & Gourgoulhon 1996). We consider two different scenarios corresponding to different configurations of the magnetic field:

(i) *Poloidal field.* For the case in which the internal magnetic field is purely poloidal and matches the dipolar field in the exterior, the ellipticity is given by Bonazzola & Gourgoulhon (1996) and Konno et al. (2000):

$$\rho_B = g\frac{R^8 B^2}{4GI_{zz}^2}\,. \tag{6}$$

According to the numerical simulations of Bonazzola & Gourgoulhon (1996), the magnetic distortion parameter g of a typical NS, which depends on both the equation of state and the magnetic field geometry, can range from 1 to 10 for a non-superconducting interior and can increase to 100–1000 for a type I superconductor in which all the magnetic field has been expelled from the superconducting core. It can take on an even greater values for type II superconducting cores or counter rotating electric currents. Following Regimbau & de Freitas Pacheco (2006a) we take $g = 520$ in the mid-range of permissible values of a type I superconducting core, corresponding to a core whose dimension represents 95 per cent of the equator radius. We take $B = 5 \times 10^{14}$ G as representative of the magnetar population, based on average observational values of soft gamma repeaters and anomalous X-ray pulsars,[6] but note that we have excluded two objects with characteristic times of 230 kyr and >1300 kyr for which dissipation of the magnetic field may have been important.

We find ellipticity $\rho_B = 4.8 \times 10^{-4}$. To have an idea of the magnitude of such deformation, we can compare this ellipticity with the ones predicted for elastic deformations of NSs. In this respect, $\rho_B = 4.8 \times 10^{-4}$ is about two orders of magnitude larger than the maximum elastic quadrupole deformation of conventional NSs (Horowitz 2010), but comparable to elastic deformations sustainable by solid strange stars, and 1–2 orders of magnitude below the upper limit derived for crystalline colour-superconducting quark matter (Owen 2005; Lin 2007). For $\rho_B = 4.8 \times 10^{-4}$, the GW emission is negligible compared to the magnetic torque and equation (4) simplifies to ($K \ll \pi^2 I_{zz} f^{-2}$):

$$\frac{\mathrm{d}E_{\mathrm{gw}}}{\mathrm{d}f} \sim Kf^3\,. \tag{7}$$

We note that for a rotation period of the order of ms, strongly magnetized relativistic winds could slow down the star in a few minutes as energy is rapidly transferred to the ejecta (Thompson, P. & quataert E. 2004; Bucciantini et al. 2007; Metzger et al. 2007). However, this effect is expected to be negligible for $B < (6-7) \times 10^{14}$G.

In theory, one could consider values up to $g = 1000$–$10\,000$ and $B = 10^{16}$ G for which GW emission would dominate in most of our frequency range ($K \gg \pi^2 I_{zz} f^{-2}$). However, this scenario would produce ellipticities of order unity, much higher than the ones typically considered for magnetic (DallOsso et al. 2009) or elastic (Owen 2005) NS deformations.

(ii) *Toroidal field.* A number of studies have suggested that the internal magnetic field B_t could be dominated by a strong toroidal component in the range 10^{15}–10^{17} G (Cutler 2002; Stella et al. 2005; DallOsso & Stella 2007; DallOsso et al. 2009), which could induce a prolate deformation with ellipticity

$$\rho_B \sim 1.6 \times 10^{-4}\left(\frac{B_t}{10^{16}}\right)^2\,. \tag{8}$$

Following DallOsso et al. (2009), we assume a pure internal toroidal field of $B_t = 10^{16}$G , with an external magnetic field of the order of 10^{14} G. B_t was deduced by Stella et al. (2005) from studies of the energetics and likely recurrence time of the 2004 December 27 event from SGR 1806-20, and is consistent with the thermal emissions observed in Anomalous X-ray Pulsars, assuming they are powered by the decay of the magnetic field (Kaminder et al. 2007). This value also supports constraints set by Vink & Kuiper (2006) on the X-ray spectra of the supernova remnants surrounding known magnetars.

In this case, both GW and magnetic dipole losses contribute to the magnetar spindown. At small frequencies ($f \lesssim 100$ Hz), the emission is dominated by the electromagnetic contribution, but above $f \sim 500$ Hz, GW emission becomes the most important process, approaching the saturation regime where spindown is purely gravitational ($K \gg \pi^2 I_{zz} f^{-2}$):

$$\frac{\mathrm{d}E_{\mathrm{gw}}}{\mathrm{d}f} \sim \pi^2 I_{zz} f\,. \tag{9}$$

Increasing B_t to 5×10^{16} G or 10^{17} G lowers the frequency at which GW emission becomes the dominant contribution to around 100 or 30 Hz.

4 GW EMISSION FROM SECULAR BAR MODE INSTABILITIES

Bar-mode instabilities associated with NS formation derive their name from the 'bar-like' deformation they induce, transforming a spheroidal body into an elongated bar that tumbles end-over-end. The highly non-axisymmetric structure resulting from a compact astrophysical object undergoing this instability makes such an object a potentially strong source of gravitational radiation (Chandrasekhar 1969, 1970; Friedman & Schutz 1978; Lai & Shapiro 1995; Brown 2000; New, Centrella & Tohline 2000; Shibata, Baumgarte & Shapiro 2000; Ou et al. 2004; Shibata & Karino 2004; Baiotti et al. 2007; Dimmelmeier et al. 2008; Ott 2009).

A system susceptible to bar-mode deformation is parametrized by the stability parameter, $\beta = T/|W|$, where T is the rotational kinetic energy and W is the gravitational potential energy.

There exist two different time-scales and mechanisms for these instabilities. Uniformly rotating, incompressible stars are *secularly* unstable if $\beta \gtrsim 0.14$, and have a growth time that is determined by the time-scale of dissipative processes in the system (such as viscosity or gravitational radiation) – usually much longer than the dynamical time-scale of the system (see e.g. Saijo et al. 2001; New et al. 2000). In contrast, a *dynamical* instability sets in when $\beta \gtrsim 0.27$, and has a growth time of the order of the rotation period of the object (see e.g. New et al. 2000). This is expected to be the fastest growing mode.

[6] The McGill SGR/AXP online catalogue can be found at http://www.physics.mcgill.ca/~pulsar/magnetar/main.html

Because bar-mode instabilities are a potentially important source of gravitational radiation, they have been the subject of many numerical studies. Dimmelmeier et al. (2008) found that the post-bounce core cannot reach sufficiently rapid rotation to become unstable to the classical high-β dynamical bar-mode instability. However, they found that many of their post-bounce core models had sufficiently rapid rotation to become subject to a low-β dynamical instability first seen by Centrella et al. (2001). The potential for enhancements in the GW emissions by dynamical instabilities at low β is encouraging and has been demonstrated in a number of other studies (Shibata, Karino & Eriguchi 2002; Ott et al. 2005; Scheidegger et al. 2008, 2010).

The requirement of rapid rotation for post-collapse instabilities suggests that a GRB progenitor, typically required to be in high rotation (Woosley & Janka 2005), may provide favourable conditions for such instabilities to set in. In this paper we follow Corsi & Mészáros (2009a,b) and consider GW emissions from the longer lived secular bar-mode instability possibly associated with the observed shallow decay phase observed in GRB X-ray afterglows discussed earlier. In the next section we describe the single source models we employ to estimate the GW backgrounds from this instability.

4.1 Single-source spectrum from secular bar-mode instabilities

The single-source emission mechanism used in this section is motivated by the study of Corsi & Mészáros (2009a) who estimated the GW emissions from a secular instability in a newly born magnetar. Their work extended the work of Lai & Shapiro (1995) for the quasi-static evolution of NSs under gravitational radiation. Treating the NS as a polytrope of index $n = 1$, they assumed typical parameter values: total mass, $M = 1.4\,\mathrm{M}_{\odot}$; radius, $R = 20$ km; initial magnetic dipole field strength at the poles, $B = 10^{14}$ G; and $\beta = 0.20$ corresponding with the middle of the expected range for the secular instability ($0.14 < \beta < 0.27$). They estimated quasi-periodic GW emissions at around 150 Hz, with characteristic amplitudes $h_{\mathrm{c}} \sim 10^{-21}$ at 10 Mpc.

Fig. 1 shows the rest-frame energy spectrum, $\mathrm{d}E_{\mathrm{gw}}/\mathrm{d}f$, from this mechanism. This function was computed through

$$\frac{\mathrm{d}E_{\mathrm{gw}}}{\mathrm{d}f} = \frac{\mathrm{d}E_{\mathrm{gw}}}{\mathrm{d}t}\left|\frac{\mathrm{d}t}{\mathrm{d}f}\right|, \tag{10}$$

using data for the luminosity and frequency evolution of the instability supplied by Corsi & Mészáros (2009a). The bulk of the emission

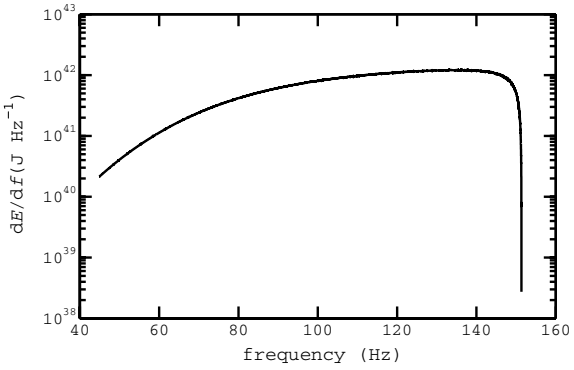

Figure 1. The rest-frame energy spectrum for GW emission by a secular bar-mode instability for parameter values $M = 1.4\,\mathrm{M}_{\odot}$; $R = 20$ km; $B = 10^{14}$ G; $\beta = 0.20$. During the first 2000 s of the evolution, the GW energy is emitted in the 50–150 Hz energy band.

takes place over the first 2000 s; during the first 100 s the GW frequency is constant at 150 Hz. This is then followed by a slow decline over about 2000 s to ∼100 Hz. Their analytical treatment included the effects of energy losses from magnetic dipole radiation. In principle, the secular evolution would bring the star to reach a stationary football configuration; thus one could follow the predicted GW signal until its frequency approaches zero. Corsi & Mészáros (2009a) conservatively shut off the bar emission after about a few thousand seconds of evolution (as for typical GRB plateau durations), when the GW signal had a frequency of about 50 Hz, and its amplitude was falling below the ALIGO sensitivity curve. We note that the ET sensitivity below 50 Hz is one order of magnitude better than for ALIGO, but the final stages of the secular evolution are indeed highly uncertain (due to e.g. viscosity effects possibly coming into play; see e.g. Lai & Shapiro 1995, Corsi & Mészáros 2009a). Thus, also in this analysis we conservatively assume that the bar emission completely shuts off on the typical duration of GRB plateaus, when the GW signal frequency is around 50 Hz.

We note here that, despite uncertainties on the values of the model parameters, Fig. 1 can be considered as an average case: mass, radius and magnetic field of the NS are chosen so as to represent the typical case for a newborn magnetar; β, is chosen to be in the middle of the secular instability range. We also stress that, as discussed in Corsi & Mészáros (2009), with this typical choice of parameters, the observed time-scale of GRB plateaus is correctly reproduced. Moreover, the amount of energy released by the magnetar for dipole losses during such time-scale is of the order of 10^{50} erg, i.e. comparable to the isotropic energy output of long sub-luminous GRBs, and thus sufficient to actually cause a visible plateau in their light curve.

5 THE GRAVITATIONAL WAVE BACKGROUND

5.1 Cosmic metallicity evolution

The spectral form of an AGB is highly dependent on the variation of the event rate with z (Howell et al. 2004; Coward, Burman & Blair 2001; Regimbau & Mandic 2008). In general, due to the relatively short lifetimes of massive stars (of the order of tens of Myr) the transient populations that produce AGBs are assumed to track the star formation rate (SFR); for transient populations of coalescing compact objects an additional factor is included to account for merger time delay. For the case of an AGB from SL-GRBs, there is growing evidence that cosmic metallicity evolution must also be considered (Li 2008; Modjaz et al. 2008).

For WR stars to retain sufficient rotation to power a GRB, angular momentum losses through stellar-wind induced mass-loss must be minimized (Woosley & Heger 2006). As wind-driven mass loss in WR stars is understood to be dependent on a high enough fraction of iron, a low-metallicity environment is an essential requirement (Vink & de Koter 2005; Woosley & Janka 2005).

To account for metallicity evolution of SL-GRBs with redshift we adopt the simple model of Langer & Norman (2006)

$$\Psi(z, \epsilon) = \frac{\hat{\Gamma}(0.84, \epsilon^2 10^{0.3z})}{\Gamma(0.84)}, \tag{11}$$

where $\epsilon = \mathrm{Z}/\mathrm{Z}_{\odot}$ is the fraction of solar metallicity and $\Psi(z, \epsilon)$ is the fraction of massive stars at z born with metallicity less than $Z_{\odot}\,\epsilon$. Here, $\hat{\Gamma}$ and Γ are the incomplete and complete gamma functions. Langer & Norman (2006) found that a metallicity cut-off of $\epsilon = 0.1$, corresponding to ∼1 GRB per 100 WR stars throughout the Universe, was able to reproduce the observed global ratio of

the rates of GRBs to core-collapse SNe. This value was also used by Salvaterra & Chincarini (2007) who suggested that luminosity evolution was required to reproduce the *Swift* distribution at high z. An analysis of the *Swift* data (to 2009 August) by Butler, Bloom & Poznanski (2010) ruled out luminosity evolution and found a more relaxed cut-off $\epsilon \sim 0.2$–0.5 was adequate to reproduce the observed sample. Their more modest dependence on metallicity was supported by studies of the mass distribution of GRB host galaxies by Kocevski, West & Modjaz (2009). Based on these studies, we adopt here a range $\epsilon \sim 0.1$–0.5 to allow for present uncertainty.

5.2 Source rate density evolution

Our source rate evolution model for SL-GRBs with redshift, $R_{\rm SL}(z)$, is obtained by scaling the star formation history,[7] $R_{\rm SF}(z)$, with the function $\Psi(z, \epsilon)$:

$$R_{\rm SL}(z) = \Psi(z, \epsilon) R_{\rm SF}(z)\,. \tag{12}$$

For $R_{\rm SF}(z)$, we employ the model of Hopkins & Beacom (2006), who constrained the SFR history by combining recent measurements taken from sources observed at ultraviolet, far-infrared and radio with previous more robust measurements taken over the last decade. By normalizing $R_{\rm SL}(z)$ to the local ($z = 0$) rate, we produce a dimensionless evolution factor

$$e(z) = R_{\rm SL}(z)/R_{\rm SL}(z=0)\,. \tag{13}$$

This allows us to extrapolate a local rate density to cosmological volumes.

5.3 The event rate equation

In order to evaluate the contribution by a population of GW sources to a stochastic background signal, knowledge of the rate of emissions from recent and past epochs is essential. The source rate evolution of an AGB is modelled by the differential event rate, $\mathrm{d}R/\mathrm{d}z$, which describes the rate of events in the redshift shell z to $z + \mathrm{d}z$:

$$\mathrm{d}R = \frac{\mathrm{d}V}{\mathrm{d}z}\frac{r_0 e(z)}{1+z}\mathrm{d}z\,. \tag{14}$$

The $(1 + z)$ factor accounts for the time dilation of the observed rate by cosmic expansion; its inclusion converts source-count information to an event rate. The parameter r_0 is the local rate density, usually defined within a volume spanning the Virgo cluster of galaxies (at around 20 Mpc). This factor is fundamental to estimating the number of potentially observable events and is determined using estimated source rates within a larger fixed volume of space. For the factor r_0, we adopt the values discussed in Section 2 of ($r_{\rm U}$, $r_{\rm P}$, $r_{\rm L}$) = (1800, 200, 40) Gpc^{-3} yr^{-1}.

The comoving volume element $\mathrm{d}V$ describes how the number densities of non-evolving objects locked into Hubble flow are constant with redshift. This is obtained by calculating the luminosity distance from (cf. Peebles 1993, p. 332)

$$d_{\rm L}(z) = (1+z)\frac{c}{H_0}\int_0^z \frac{\mathrm{d}z'}{h(z')}\,, \tag{15}$$

and using equation (3) of Porciani & Madau (2000),

$$\frac{\mathrm{d}V}{\mathrm{d}z} = \frac{4\pi c}{H_0}\frac{d_{\rm L}^2(z)}{(1+z)^2\,h(z)}. \tag{16}$$

[7] In units of mass converted to stars per unit time and volume.

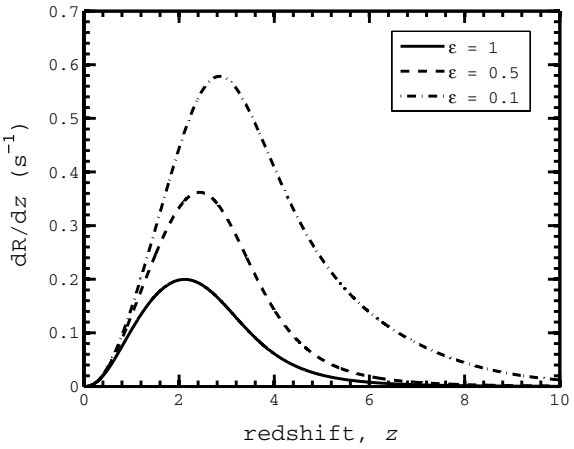

Figure 2. The differential event rate $\mathrm{d}R/\mathrm{d}z$ of SL-GRBs as a function of redshift based on the SFR model of Hopkins & Beacom (2006). The three curves correspond to different metallicity cut-offs $\epsilon = (0.1; 0.5; 1)\,\mathrm{Z}_\odot$ at the upper rate estimate of $r_{\rm U} = 1800\,\mathrm{Gpc}^{-3}\,\mathrm{yr}^{-1}$. Inclusion of cosmic metallicity evolution increases the contribution from sources at higher z. This is shown by a shift in the peak of $\mathrm{d}R/\mathrm{d}z$ from $z \sim 2$ ($\epsilon = 1$) to $z \sim 3$ assuming SL-GRBs follow a low-metallicity dependence of $\epsilon = 0.1\,\mathrm{Z}_\odot$.

The normalized Hubble parameter, $h(z)$, is given by

$$h(z) \equiv H(z)/H_0 = [\Omega_{\rm m}(1+z)^3 + \Omega_\Lambda]^{1/2}\,, \tag{17}$$

for a 'flat-Λ' cosmology. We take $\Omega_{\rm m} = 0.3$, $\Omega_\Lambda = 0.7$ and $H_0 = 70$ km s^{-1} Mpc^{-1} for the Hubble parameter at the present epoch (Rao, Turnshek & Nestor 2006).

Fig. 2 shows the form of $\mathrm{d}R/\mathrm{d}z$ assuming different metallicity cut-offs for SF-GRBs. In this plot we compare curves corresponding to the different cut-offs $\epsilon = (0.1, 0.5)$ with the $\epsilon = 1$ solar metallicity curve. The inclusion of cosmic metallicity evolution increases the contribution from higher-z sources, shown by a shift of the peak from $z \sim 2$ to $z \sim 3$ for a low-metallicity dependence, $\epsilon = 0.1\,\mathrm{Z}_\odot$. The magnitude of the peak value also increases by up to a factor of 3. Thus, the additional contribution from sources at higher z should enhance the lower frequency component of the stochastic background signal through redshift.

5.4 The Gravitational wave background spectra

The spectral time-integrated flux density or spectral fluence, in J m^{-2} Hz^{-1}, of a quadrupole GW signal at a luminosity distance $d_{\rm L}(z)$ from a single source can be expressed as

$$F_{\rm ss}(f_{\rm obs}, z) = \frac{\mathrm{d}E_{\rm gw}(f_{\rm obs})}{\mathrm{d}f}\,\frac{(1+z)}{4\pi d_{\rm L}(z)^2}\,, \tag{18}$$

where $\mathrm{d}E_{\rm gw}(f_{\rm obs})$ is the spectral GW energy at the observed frequency $f_{\rm obs}$, which is related to the source frequency f by the redshift factor: $f_{\rm obs} = f/(1+z)$.

The background spectral flux density, in W m^{-2} Hz^{-1}, from all events throughout the Universe is obtained by integrating the product $F_{\rm ss}(f_{\rm obs}, z)\,\mathrm{d}R/\mathrm{d}z$ over the redshift range $z = 0$ to $z_{\rm lim}$:

$$F_B(f_{\rm obs}) = \int_0^{z_{\rm lim}} [\,F_{\rm ss}(f_{\rm obs}, z)(\mathrm{d}R/\mathrm{d}z)\,]\,\mathrm{d}z\,, \tag{19}$$

with the integrand given by (14) and (18) within a limiting redshift, $z_{\rm lim} = 10$, which we take as the beginning of stellar activity. In support of this value we note that GRB 090423, the most distant recorded burst ($z = 8.2$), showed no evidence of properties that

were inconsistent with the majority of the observed GRB population (Tanvir et al. 2009).

The spectral energy density of a GW background is conventionally expressed by the dimensionless energy density parameter, $\Omega_{\rm B}(f_{\rm obs})$, defined as the energy density of GWs per logarithmic frequency interval normalized to the cosmological critical energy density $\rho_{\rm c} = 3H_0^2/8\ \pi G$. This function can be constructed from $F_{\rm B}(f_{\rm obs})$ (Ferrari, Matarrese & Schneider 1999a; Howell et al. 2004; Regimbau & Mandic 2008):

$$\Omega_{\rm B}(f_{\rm obs}) = f\ F_B(f_{\rm obs})/(\rho_{\rm c}c^3)\ . \tag{20}$$

Throughout this paper we will present our estimated GW background spectra using this function.

5.5 The duty cycle of an astrophysical GW background

When we consider AGB signals, in addition to the energy density and characteristic frequency, another useful quantity is the duty cycle (*DC*) (Blair & Ju 1996; Maggiore 2000; Coward & Regimbau 2006; Regimbau & Mandic 2008). The value of the *DC* is given by the ratio of the typical duration of the signal, τ, to the average waiting time between the reception of successive events. The waiting time will depend on the rate of events as observed in our frame, R, and thus a *DC* is generally defined by the quantity $R \times \tau$. When considering a cosmological distribution of events, the *DC* is determined by sources within a limiting redshift, $z_{\rm lim}$:

$$DC(z_{\rm lim}) = \int_0^{z_{\rm lim}} (1+z)\tau({\rm d}R/{\rm d}z)\,{\rm d}z\ . \tag{21}$$

Here, the signal duration is dilated to $(1+z)\tau$ by the cosmic expansion and the quantity ${\rm d}R/{\rm d}z$ is the cosmologically dependent differential event rate given by equation (14).

Many studies are concerned with the value of *DC* as seen at the detector and determine the value of *DC* by setting $z_{\rm lim}$ equal to the redshift at which stellar activity began. In this case equation (21) provides a total value, $DC(z_{\rm lim})$. As source rate evolution will increase out to large cosmological volumes, it is interesting to see how *DC* too increases with z. In this study, we will therefore calculate *DC* as a function of redshift.

In general, for an AGB the signal is defined as continuous if it has a *DC* of unity or above. As it will still be possible to resolve individual events in this regime, a more conservative threshold can be defined from the view of single detections as $DC \geq 10$ (see Regimbau & Hughes 2009). Thus, using the convention of Regimbau & de Freitas Pacheco (2006b), non-continuous signals can be further categorized into shot and popcorn type. More descriptive definitions of these components are provided as follows.

Continuous ($DC \geq 10$). This signal is, at any given time, the superposition of a large, but random, number of overlapping signals. As the amplitude of each contributing signal is itself random, the central limit theorem will apply leading to a Gaussian distribution in amplitudes. Because it will be difficult to resolve the individual components, this signal can potentially mask a background signal of primordial origin (Maggiore 2000). For this reason, AGB with $DC \geq 10$ would be bad news from the perspective of primordial background searches.

Popcorn noise ($0.1 \leq DC < 10$). This signal will manifest in GW data as a non-continuous stochastic background signal with an amplitude distribution dependent on the spatial distribution of the sources. For background signals with *DC*s at the lower end of the popcorn noise range, the individual components will rarely overlap. In this case the signal will be dominated by the closest events of a population of sources.

Shot noise ($DC < 0.1$): For this signal, the waiting time between events is large in comparison with the duration of a single event (Regimbau & de Freitas Pacheco 2006b).

Using these three definitions of *DC*, Coward & Regimbau (2006) have shown that an AGB can be divided into three different detection regimes, each defined by the corresponding shells of $z_{\rm lim}$. For most types of AGB, at low z, the signal produced is predominantly of the shot-noise type, extending to popcorn and continuous with z, due to time dilation and increased source rate density. The weighting of the different AGB regimes for a particular source population depends strongly on the event rate and is an important consideration when selecting the most appropriate signal detection strategy.

6 DETECTION

In this study we consider the design sensitivities of second-generation interferometric detectors, such as ALIGO[8] (expected online in 2015) and Virgo,[9,10] and third-generation ones, for which we will use ET[11] (possible construction will be late in the next decade).

For ALIGO, we use the sensitivity curve based on the zero detuning, high laser power configuration.[12] For ET we consider two target sensitivities. First, ET-B, which is an underground-based design, incorporating long suspensions, cryogenics and signal and power recycling (Hild, Chelkowski & Freise 2008). Secondly, a so-called *Xylophone* configuration, ET-C, which merges the output of two detectors specializing in different frequency bands: (a) an underground low-frequency cryogenic configuration with long suspensions and moderate laser power; (b) a high-frequency detector implementing squeezed light states, large test masses and a high power laser (Hild et al. 2010). The advantage of this strategy is that it can decouple the obstacles in operating a high power laser alongside a cryogenically cooled suspension optimized for thermal noise (Shoemaker 2001). The design sensitivity curves for these four detectors are shown in Fig. 3.

The most promising detection strategy for continuous GW background signals is cross-correlating the output of two neighbouring detectors (see Maggiore 2000; Allen & Romano 1999). For this strategy to be achieved, the detectors must be separated by less than one reduced wavelength, which is about 100 km for frequencies around 500 Hz where $\Omega_{\rm B}(f)$ might peak. The detectors also need to be sufficiently well separated that their noise sources are largely uncorrelated. We note that although this may not be possible for ET, techniques are in development to remove environmental noise and instrumental correlations (Fotopoulos 2008).

Under these conditions, assuming Gaussian noise in each detector and optimal filtering, a filter function chosen to maximize the signal-to-noise ratio (S/N) for two such detectors is given by (Allen &

[8] http://iopscience.iop.org/0264-9381/27/8/084006

[9] https://pub3.ego-gw.it/codifier/includes/showTmpFile.php?doc=2219&calledFile=VIR-027A-09.pdf

[10] www.virgo.infn.it

[11] A 3-year design study for the Einstein GW telescope began in 2008 May. For details see http://www.ego-gw.it/ILIAS-GW/FP7-DS/fp7-DS.htm, 'Design Study Proposal for E.T. (Einstein Gravitational Wave Telescope)', submitted to the EU Seventh Framework Programme.

[12] The ALIGO sensitivity curve is described in the public LIGO document LIGO-T0900288-v2 (https://dcc.ligo.org/public/0002/T0900288/002/AdvLIGO noise curves.pdf).

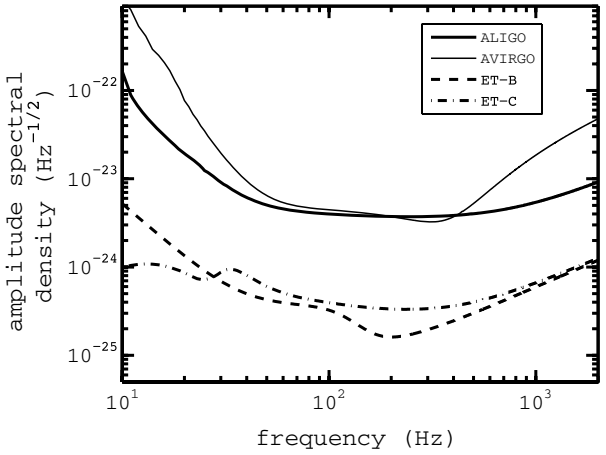

Figure 3. The design sensitivity curves for advanced LIGO (ALIGO), Advanced Virgo (AVIRGO) and two possible configurations of the third-generation ET: ET-B and ET-C (see Section 7 for more details).

Romano 1999, eq.3.75)

$$\left(\frac{\mathrm{S}}{\mathrm{N}}\right)^2 \approx \frac{9H_0^4}{50\pi^4} T \int_0^\infty \frac{\gamma^2(f)\Omega_\mathrm{B}^2(f)}{f^6 S_{n1}(f) S_{n2}(f)}\,\mathrm{d}f\,. \tag{22}$$

Here, $\gamma(f)$ is the 'overlap reduction function', which accounts for the separation and relative orientation of the detectors, and $S_{n1}(f)$ and $S_{n2}(f)$ are the noise power spectral densities of the detectors; T is the integration time. As the optimal filter depends on $\Omega_\mathrm{B}(f)$, a range of filter functions based on theoretical expectations of this function will need to be used. In this study we adopt a value of $\mathrm{S/N} = 3$ to indicate detection, corresponding with false alarm rate of 10 per cent and detection rate of 90 per cent (Allen & Romano 1999).

For signals of the shot noise and popcorn type, the standard cross-correlation strategy in the frequency domain may not be optimal and other methods in the time domain have been proposed or are currently under investigation in the LIGO-Virgo collaboration (Drasco & Flanagan 2003; Coward & Burman 2005). For signals of the shot noise type, individual events may be clearly distinguishable and, if within a detector's range, can potentially be resolved using data analysis techniques such as matched filtering.

To estimate the detectability of the GW backgrounds considered in this paper we will assume continuous signals, and hence use the cross-correlation statistic to determine S/N. For cases in which a significant proportion of the background signal will not be continuous, we will also investigate the different z regimes in which the shot, popcorn and continuous regimes exist. We calculate the S/N for the two generations of GW detector outlined above; for second-generation we assume 3 years of integration by an ALIGO configuration; for third generation we assume 1 year of integration by (ET-B; ET-C). We further assume: (a) separated detectors; (b) an optimal case in which a pair of equivalent detectors is situated within several km and aligned. For ALIGO we will employ the LIGO Hanford/Livingston pair (H1-L1) for scenario (a), using for $\gamma(f)$ the form given by equation (3.26) of Allen et al. (2002). For ET we assume two detectors located in Cascina, of triangular shape (60° between the two arms) and separated by an angle of 120°. In the frequency range we are interested in (1–1000 Hz), $\gamma(f)$ reduces to a value of –3/8. For case (b) we will assume $\gamma(f) = 1$ for both second- and third-generation detectors.

For convenient comparison of $\Omega_\mathrm{B}(f)$ with the GW interferometric sensitivity curves discussed above, the noise power spectrum, $S_\mathrm{n}(f)$ (in units of Hz^{-1}), over a frequency range Δf can be expressed in terms of a detector energy density, $\Omega_\mathrm{det}(f)$, over an integration time T_int:

$$\Omega_\mathrm{det}(f) = \frac{50\pi^2}{3H_0^2} \frac{S_\mathrm{n}(f)}{\Delta f\, T_\mathrm{int}\, \gamma(f)}\, f^3\,. \tag{23}$$

The sensitivity curves will be presented for the optimal scenario (b), as discussed above for integration times of 1 and 3 years for ET and ALIGO, respectively.

7 THE GW BACKGROUND FROM NEWLY FORMED MAGNETARS

Figs 4 to 6 show the function $\Omega_\mathrm{B}(f_\mathrm{obs})$ from triaxial deformations in magnetars associated with SL-GRBs for the three mechanisms discussed in Section 3. Curves are displayed at the rates (r_U, r_P, r_L) and metallicity cut-offs $\epsilon = 0.1$ (thick lines) and $\epsilon = 0.5$ (thin lines). Each plot also includes the detector sensitivities of ALIGO and ET-B assuming 3 years of integration.

Fig. 4 shows the function $\Omega_\mathrm{B}(f_\mathrm{obs})$ assuming that the internal magnetic field is purely poloidal and matches to the external dipole field. For this case, the GW emission is negligible in comparison with the magnetic torque and the gravitational signal increases as f^4 until a maximum at around 840 Hz for rate r_U. We see that the signal is outside the sensitivity of ET, and even at the most optimistic rates this background would not be detected within a reasonable integration time. For higher values of B or ellipticity and smaller values of I_{zz}, the amplitude increases until the GW emission dominates ($\Omega \sim f^2$) at large frequencies (see Fig. 5), eventually reaching a saturation regime (Fig. 6).

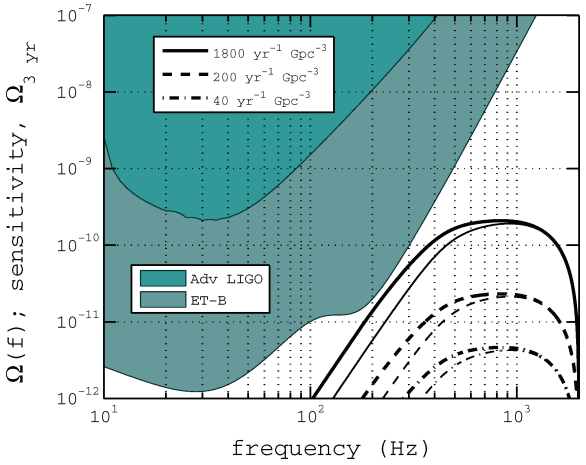

Figure 4. The GW background spectrum from triaxial deformations in newly born magnetars associated with SL-GRBs in the regime where the spindown is dominated by the magnetic torque. The three curves assume that triaxial deformations are introduced by an internal poloidal magnetic field ($B = 5 \times 10^{14}$G; $g = 520$; $I_{zz} = 10^{45}\,\mathrm{kg\,m^2}$; $R = 10\,\mathrm{km}$). The curves are presented for three rates of occurrence: (r_U, r_P, r_L) = (1800, 200, 40) $\mathrm{Gpc^{-3}\,yr^{-1}}$ and metallicity cut-offs of $\epsilon = 0.1$ (thick curves) and $\epsilon = 0.5$ (thin curves). The sensitivity curves of second- and third-generation laser interferometric detectors are represented by ALIGO and ET-B, in terms of $\Omega_\mathrm{det}(f)$ assuming a 3 year integration. Based on observational values of SGRs and anomolous X-ray pulsars, we assume the value of B used here is representative of the magnetar population. This value gives $\rho_B = 4.8 \times 10^{-4}$, comparable to elastic deformations sustainable by solid strange stars, and 1–2 orders of magnitude below the upper limit derived for crystalline colour-superconducting quark matter.

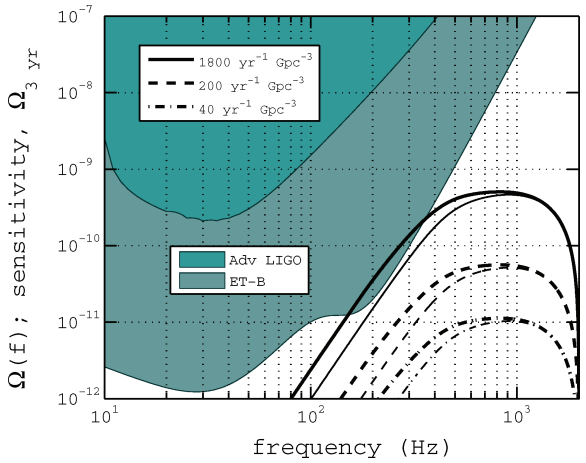

Figure 5. As for Fig. 4, but in the regime where both magnetic and GW emission contribute to the spindown. The triaxial deformations are produced by an internal toroidal field ($B_t = 10^{16}$ G; $B = 10^{14}$ G).

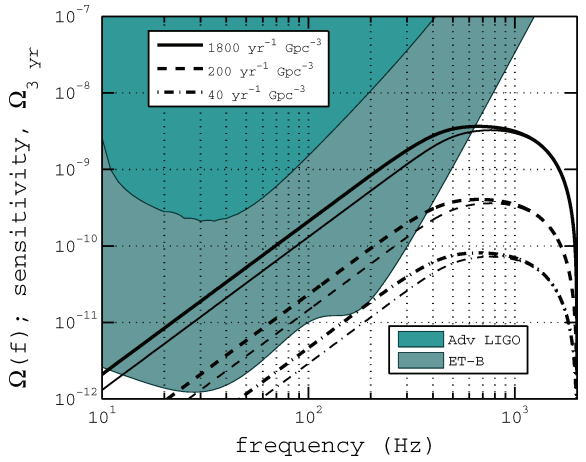

Figure 6. As for Fig. 4 but showing upper limits on the GW background spectrum from triaxial deformations in newly born magnetars associated with SL-GRBs. The three curves assume a pure gravitationally induced spindown as given by equation (9) with $I_{zz} = 10^{45}$ kg m^2. We note that in this case, Ω depends linearly on I_{zz} and is independent of the ellipticity.

Fig. 5 displays the function $\Omega_B(f_{obs})$ assuming that internal toroidal fields contribute towards a prolate distortion. For this case, both GW and magnetic dipole emissions contribute to the spindown. We see that for the upper rate r_U and $\epsilon = 0.1$ the signal peaks at $\Omega_B(f_{obs}) \sim 5 \times 10^{-10}$ at around 830 Hz. Even at this upper rate only a small part of this signal is within the sensitivity of ET-B.

In Fig. 6, we show the upper limit in which spindown is purely gravitational (from equation 9). We see that the background signal increasing with f^2 and reaching a maximum $\Omega_B(f_{obs}) \sim 4 \times 10^{-8}$ at around 660 Hz for rate r_U. In this case, Ω depends linearly on I_{zz} and is independent of the ellipticity.

As illustrated by the thin lines for each curve, which represent $\epsilon = 0.5$, we see that a more relaxed metallicity cut-off results in a smaller contribution below the peak, and hence, a lower S/N, as will be shown below.

Tables 3 and 4 display the S/N for the three AGBs considered in this section for metallicity cut-offs of $\epsilon = 0.1$ and 0.5, respectively. Estimates are shown for $r_P = 200\,\mathrm{Gpc^{-3}\,yr^{-1}}$. Values for the rates $(r_U; r_L) = (1800;40)\,\mathrm{Gpc^{-3}\,yr^{-1}}$ can be obtained through the ratios (200/1800; 200/40). For a GW background produced by

Table 3. The S/N obtained through cross-correlation for a GW background of triaxially deformed newly born magnetars associated with SL-GRBs for an event rate of $r_P = 200\,\mathrm{Gpc^{-3}\,yr^{-1}}$. Values for the other rates considered in this study, $(r_U; r_L) = (1800;40)$, $\mathrm{Gpc^{-3}\,yr^{-1}}$, can be obtained through the ratios (200/1800; 200/40). A metallicity cut-off of $\epsilon = 0.1$ is assumed for SL-GRBs. These tabulated values assume 3 years of integration by cross-correlation of data from two detectors. We also assume the overlap reduction functions described in section 5 – values obtained by optimally orientated and co-located detectors are shown in parentheses. The S/N obtained from the two emission scenarios considered in Section 3 are shown: distortions induced by poloidal fields and toroidal fields; in addition we show upper limits that assume spindown is solely gravitational. We note that the pure GW upper limit could increase up to three times the values shown above, as I_{zz} can be one to three times the canonical value used in this study (Ruderman 1972).

Emission mechanism	ALIGO	ET-B	ET-C
Poloidal field	1×10^{-5}	0.08	0.03
	(6.1×10^{-4})	(0.07)	(0.1)
Toroidal field	2.5×10^{-5}	0.2	0.07
	(1.5×10^{-3})	(0.5)	(0.2)
Pure GW spindown	0.006	4.5	1.7
	(0.04)	(12.0)	(4.6)

Table 4. As for Table 4 but with a metallicity cut-off of $\epsilon = 0.5$ for SL-GRBs.

Emission mechanism	ALIGO	ET-B	ET-C
Poloidal field	4.2×10^{-6}	0.04	0.01
	(3.4×10^{-4})	(0.1)	(0.04)
Toroidal field	1.1×10^{-5}	0.1	0.04
	(8.5×10^{-4})	(0.3)	(0.1)
Pure GW spindown	0.004	2.8	1.3
	(0.03)	(7.6)	(3.4)

toroidal field induced distortions, as illustrated in Fig.5, at the upper rate r_U a small part of this signal is within the sensitivity of ET-B. This produces a S/N of 1.8 for 3 years of integration. Optimistically, for an upper limit AGB from pure GW spindown, the S/N confirm that detection would require a third-generation detector. Assuming a metallicity cut-off of $\epsilon = 0.1$, we find that source rates of $(133;349)\,\mathrm{Gpc^{-3}\,yr^{-1}}$ would result in detection by (ET-B, ET-C) within 3 years at a S/N of 3. A more relaxed metallicity cut-off, $\epsilon = 0.5$, increases the corresponding rates required for detection to $(210;552)\,\mathrm{Gpc^{-3}\,yr^{-1}}$. As shown in Table 4 we see that ET-C, which is optimized for greater sensitivity at low frequency, $\leq$20 Hz, does not improve on the S/N of ET-B. We note that this final scenario can be regarded only as an upper limit, but we consider it as it could allow ET to place constraints on this source population.

We note that in general, independent of the particular mechanism driving the deformation, an NS with an ellipticity ρ_B and an external field B will emit GWs according to equations (4) and (5). The S/N for the corresponding GW background signal will therefore depend on the combination ρ_B/B. Treating ρ_B and B as

Table 5. The minimal value of the product $(\rho_B/10^{-4})(B/10^{14})^{-1}$ required to obtain an S/N of 3 with ET-B over 3 years of observation, for the three rates considered in this paper and for metallicity cut-offs of $\epsilon = 0.1$ and $\epsilon = 0.5$. An omitted value implies that a detection is not expected.

Rate ($\mathrm{Gpc^{-3}\,yr^{-1}}$)	$\epsilon = 0.1$	$\epsilon = 0.5$
40	–	–
200	15	Pure GW
1800	2	3

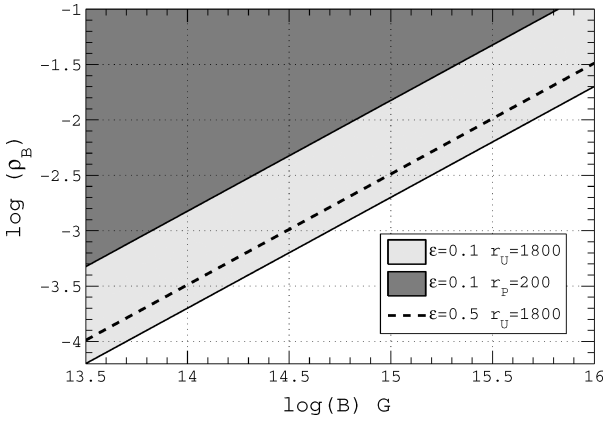

Figure 7. The $\rho_B - B$ plane accessible by ET-B for magnetars associated with SL-GRBs. The shaded zones, set by the product $(\rho_B/10^{-4})(10^{14}/B)$, show the parameter space that can be explored for different values of the rate and metallicity ϵ.

independent parameters, and assuming that the NS is born in association with SL-GRB, we can make a statement on detectability that is independent of the actual mechanism causing the ellipticity. This is done in Table 5 by computing, for each value of the rate (r_L, r_P, r_U) and of the metallicity cut-off ϵ, the minimum $(\rho_B/10^{-4})(10^{14}/B)$ required to have a detection with a given detector configuration. The full parameter space is illustrated in Fig. 7, for which the product $(\rho_B/10^{-4})(10^{14}/B)$, shown by the diagonal lines in the $\rho_B - B$ plane, divides the plot into detectibility zones (shown by the legend). We see that for a rate of r_L even pure GW emission is out of reach. However, with r_P we could access extreme values and with r_U a large part of parameter space is detectable.

In the next section, we will consider the background signal from secular instabilities which occur on a shorter time-scale than the emissions considered in this section, $\sim$1000 s, corresponding with the X-ray plateaus observed in some LGRBs. For this signal some analysis of the *DC* will be important.

8 THE GW BACKGROUND FROM SECULAR BAR-MODE INSTABILITIES

8.1 The GW background spectrum

The S/N estimated for a background signal from secular bar mode instabilities in SL-GRBs are shown in Tables 6 and 7 for the rates (r_U, r_P, r_L). The estimates indicate that ALIGO will require 3 yr of integration by optimally orientated and co-located detectors to reach

Table 6. The S/N achievable through cross-correlation of 3 yr of data by ALIGO and 1 yr by ET-B or ET-C, for a GW background resulting from secularly unstable magnetars associated with SL-GRBs. Values are shown for the rates $(r_U, r_P, r_L) = (1800, 200, 40)\,\mathrm{Gpc^{-3}\,yr^{-1}}$ and assume a metallicity cut-off $\epsilon = 0.1$. The S/N estimates assume the overlap reduction functions described in Section 6 – values obtainable by optimally orientated and co-located detectors are shown in parentheses.

Rate $\mathrm{Gpc^{-3}\,yr^{-1}}$	ALIGO	ET-B	ET-C
1800	1 (4)	113 (300)	67 (178)
200	0.1 (0.4)	13 (33)	8 (20)
40	0.02 (0.08)	3 (7)	2 (4)

Table 7. As for Table 6 but with a metallicity cut-off of $\epsilon = 0.5$ for SL-GRBs.

Rate $\mathrm{Gpc^{-3}\,yr^{-1}}$	ALIGO	ET-B	ET-C
1800	0.7 (3)	96 (257)	55 (148)
200	0.09 (0.3)	11 (29)	6 (16)
40	0.02 (0.07)	2 (6)	1 (3)

a S/N of 1 for the optimistic rate r_U. For ET-B, however, this signal can potentially be detected with a S/N ≥ 3 in the more conservative hypothesis for SL-GRB rates r_L and detector performances.

We stress here that these estimates are based on two main assumptions:

(i) that at least 40 per cent of SL-GRBs are associated with magnetar progenitors undergoing a secular bar-mode instability;
(ii) that the magnetar's parameters are those adopted to calculate the single-source spectrum shown in Fig. 1.

Regarding (i), we note that there is significant uncertainty in how often SL-GRBs could be associated with a secularly unstable magnetar progenitor. This, in turn, implies a large uncertainty on our rate estimates. To address this problem, we have chosen a wide range of values.

We note again that our lower rate r_L accounts for the fraction of LGRBs showing X-ray plateaus in the *Swift* Era – around 40 per cent (Evans et al. 2009). We suggest that r_L is a reasonable estimate also in view of the uncertainty (ii) underlined above. In fact, the parameter values adopted by Corsi & Mészáros (2009a) aimed at explaining the typical case of a $\sim$1000 s duration plateau observed in a LGRB with an energy release similar to those of SL-GRBs. It is thus more conservative to assume that the spectrum shown in Fig. 1 would be realized only in a fraction of SL-GRBs similar to the one of LGRBs showing a plateau ($\sim$40 per cent). We note that fraction could be higher in SL-GRBs, since dipole energy injection from a magnetar can more easily cause visible plateaus on less energetic GRBs. However, it is not yet clear whether or not X-ray plateaus are always caused by a magnetar – see e.g. Panaitescu (2008) for an alternative explanation. In the light of these uncertainties, we consider r_L as a safer estimate.

We calculate that rates of $(48, 80)\,\mathrm{Gpc^{-3}\,yr^{-1}}$ for (ET-B, ET-C) are required to achieve a S/N of 3 for 1 year of integration by separated detectors. For our conservative rate r_L, (ET-B, ET-C) will require (1.4, 4) yr of integration.

Fig. 8 shows the quantity $\Omega_B(f_{obs})$ for the rates (r_U, r_P, r_L), in comparison with the sensitivity curves for second- and third-generation GW interferometric detectors represented by ALIGO and ET-B. The stochastic background signal has a frequency bandwidth 5–150 Hz with a peak of $\Omega_B(f_{obs}) \sim 10^{-9}$ at around 80 Hz. The thin lines in the figure show the function $\Omega_B(f_{obs})$ assuming a more relaxed allowance for metallicity, $\epsilon = 0.5$. This illustrates once again how a lower metallicity cut-off results in a greater contribution of $\Omega_B(f_{obs})$ at lower frequency. In Appendix A we will further discuss the effect of cosmic metallicity on the GW background signal.

Fig. 9 compares the function $\Omega_B(f_{obs})$ with ET-C. In comparison with Fig. 8, we see that at the conservative rate, r_L, the only significant contribution from this signal is from $\gtrsim$50 Hz. As can be seen by a comparison of Tables 5 and 6, this results in a S/N of around a factor of 2 less. At the plausible rate r_P there is no contribution below ∼15 Hz. Therefore, for the most probable rate estimates, ET-C could still pursue a primordial GW background signal at its most sensitive frequency bandwidth.

For ET-B, this signal occurs in the most sensitive frequency regime; a largely continuous signal could therefore mask any primordial GW background signal with $\Omega(f) \leq 10^{-9}$ within the bandwidth 20–100 Hz. A *DC* analysis will indicate what proportion of sources will contribute to a continuous signal. This will have implications on both stochastic searches and single detections by ET, for which the detection horizon may enter the $DC \geq 10$ confusion limited regime. We shall investigate this in the next section.

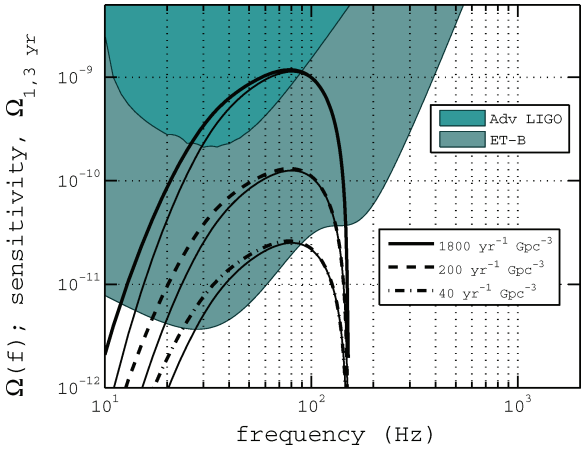

Figure 8. Upper limits on the GW background spectrum from secularly unstable magnetars associated with under-luminous GRBs for the rates $(r_U, r_P, r_L) = (1800, 200, 40)\,\mathrm{Gpc^{-3}\,yr^{-1}}$. The sensitivity curves of (ALIGO, ET-B) are shown in terms of $\Omega_{det}(f)$ and assume (3, 1) yr of integration and optimally orientated and co-located detectors. The thin curves show the background estimates for a more relaxed metallicity dependence, $\epsilon = 0.5$.

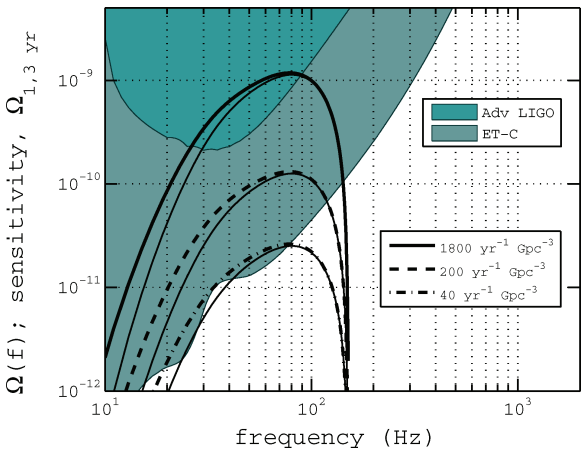

Figure 9. As for Fig. 8, but showing an alternative configuration for the Einstein Telescope, ET-C.

8.2 The duty cycle

For a GW from triaxial deformations in magnetars associated with SL-GRBs we find that for rates $(r_U, r_P, r_L) = (1800, 200, 40)\,\mathrm{Gpc^{-3}\,yr^{-1}}$ sources outside a volume defined by $z \sim (0.07, 0.1, 0.2)$ contribute to a continuous signal. This is the result of a long duration, $\tau \sim 10^6$ s in equation (21) (Stella et al. 2005).

Fig. 10 shows the duty cycle as a function of redshift for a GW background resulting from secularly unstable magnetars occurring in SL-GRBs. For τ, we use a value of 1000 s – this approximates to the typical duration of an X-ray plateau for a GRB. The plot shows that as the rate decreases, the continuous contribution to the background is from sources at greater distances. For the rates $(r_U, r_P, r_L) = (1800, 200, 40)\,\mathrm{Gpc^{-3}\,yr^{-1}}$ we find a $DC \geq 10$ is reached at around $z \sim (0.5, 1.0, 1.6)$. Therefore, sources outside volumes defined by these z values will contribute to a continuous background signal. Curves for a more relaxed cut-off $\epsilon = 0.5$ are shown by the thinner lines. Referring to Fig. 2, we see that the effect of metallicity dependence is small within $z \sim 1$. This is reflected in the curves of Fig. 10.

The optimal and isotropic (orientation-averaged) horizon distances (see Regimbau & Hughes 2009; Dalal et al. 2006, for further definitions) are greatest for the ET-B detector, at distances of $z = (0.2, 0.12)$, both less than the redshift range in which the signal becomes continuous. Thus, a confusion-limited background will not affect the resolution of individual sources.

Fig. 11 shows again the results of Fig. 8, but with thick curves to show the continuous contributions to the AGB signal from sources at z greater than (0.5, 1.0, 1.6). We see that even if the popcorn and shot components can be identified, the continuous part of the AGB could mask a primordial GW background signal in the most

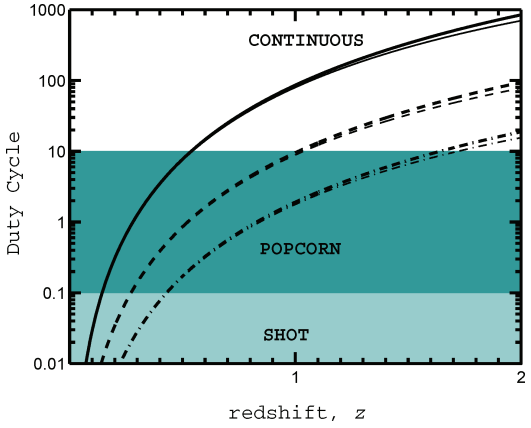

Figure 10. Duty cycle as a function of redshift for a GW background from secularly unstable magnetars in SL-GRBs occurring at rates of (40, 200, 1800) $\mathrm{Gpc^{-3}\,yr^{-1}}$. The shaded areas show three zones of an AGB corresponding to different regimes of *DC*: continuous ($DC \geq 10$), popcorn ($0.1 \leq DC < 10$) and shot noise ($DC \leq 0.1$) (Coward & Regimbau 2006). We see that sources beyond ($z = 0.5, 1.0, 1.6$) contribute to a continuous signal.

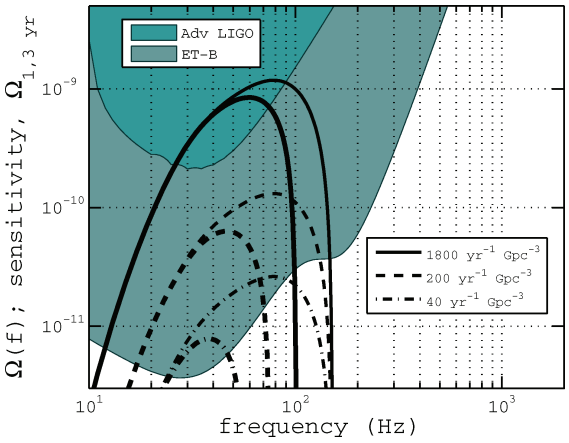

Figure 11. As for Fig. 8, but with thick lines showing only the continuous contribution ($DC \geq 10$) from sources ($z \geq 0.5$, $z \geq 1.0$, $z \geq 1.6$) for the rate estimates (r_U, r_P, r_L).

sensitive frequency regime, around 20–30 Hz, of ET-B. As rates increase, so does the continuous proportion of the AGB signal.

9 CONCLUSIONS

In this paper we have assessed the GW detection prospects for the background signals associated with SL-GRBs, assuming that the central engines of a significant proportion of these bursts are provided by newly born magnetars. We have considered two plausible GW single-source emission mechanisms: (a) the deformation-induced GW emission from a newly born magnetar and (b) the onset of a secular bar-mode instability. The latter mechanism would correspond well with the long-lived shallow plateau observed in the X-ray afterglows of many GRBs.

We have calculated the GW background spectra of each of the mechanisms by employing appropriate models for each. We account for GRBs preference towards low-metallicity environments by using a source rate history model that allows for cosmic metallicity evolution. We assume both a low-metallicity cut-off defined by $\epsilon = 0.1$ and a more relaxed cut-off, $\epsilon = 0.5$.

Our results for the deformation-induced GW emission from a newly born magnetars are more pessimistic than those presented by Regimbau & Mandic (2008). This is due to the fact that whilst they considered the emission from the population of magnetars assuming they represented 10 per cent of the population of newborn NSs [a rate of around (3–15) $\times$ 10^3 Gpc^{-3} yr^{-1}], we consider only magnetars associated with SL-GRBs.

For an AGB from triaxial emissions in newly formed magnetars associated with SL-GRBs, for an upper limit case in which emission is purely from GW emission, rates of (52, 137) Gpc^{-3} yr^{-1} will be required for detection at an S/N of 3 within 1 year by (ET-B, ET-C). For an AGB resulting from toroidal fields, an upper rate $r_U = 1800$ Gpc^{-3} yr^{-1} would produce an S/N of 1.8 after 3 years of integration by ET-B. We find, however, that rates above 200 Gpc^{-3} yr^{-1} would enable ET-B to explore the $\rho_B - B$ parameter space of the magnetar population considered in this study.

In terms of detectability, we find that an AGB resulting from the onset of a secular instability is a more optimistic scenario. We note, however, that this is highly dependent on the rate of occurrence of this instability. Using the single-source GW emission model of Corsi & Mészáros (2009a), we find that event rates of (48, 80) Gpc^{-3} yr^{-1} are sufficient to produce a detectable signal for ET (ET-B, ET-C) with S/N of 3 for 1 yr of observation. For ALIGO, detection within 3 years would require the upper limit rate estimate r_U, combined with a pair of optimally orientated and co-located detectors. We note that observations of a larger number of SL-GRBs (e.g. by future satellites like Janus or EXIST; Stamatikos et al. 2009; Imerito et al. 2008), will help in reducing the uncertainties on their local rate estimates, thus clarifying the prospects of detectability of an associated GW background.

We find that this signal could potentially mask a primordial GW background signal. The analysis of the *DC* for the background signal from secularly unstable magnetars showed that even at a conservative rate estimate r_L, a significant proportion of this signal would be continuous. As highlighted in Fig. 11, this would occur in the most sensitivity bandwidth of ET-B. Depending on the rate of occurrence, both mechanisms could produce GW backgrounds that could mask a primordial GW background signal of the order of $\Omega_B(f) \sim 5 \times 10^{-11}$ in the frequency regime 10 – 50 Hz of ET-B and ET-C. This would pose a particular problem for the former, as it is the most sensitive bandwidth of this detector.

The AGB may form a composite signal with an AGB from NS/NS inspirals, which is expected across a bandwidth of 10–800 Hz with increasing Ω_B (Regimbau & de Freitas Pacheco 2006b). As the latter background will peak at $\sim$1000 Hz, detecting the higher frequency component may enable the two AGBs to be disentangled.

To calculate S/N we have applied equation (22), which assumes the background signals can be detected through cross-correlation. We have chosen to adopt this convention for easy comparison with other AGB estimations, many of which will contain popcorn or shot noise components. In practice, to detect the non-continuous components of a GW background some other strategy will be required. Given the long duration and quasi-periodicity of the signal from secular instabilities, ET could detect a significant number of the shot noise events through matched filtering. This provides an additional means to interrogate the higher energy, shot noise and popcorn components of the background signal which result from the rarer nearby events. A statistical procedure, such as the 'probability event horizon' technique, which extracts the observation time dependence from a population of cosmological transients could be used (Coward & Burman 2005). This technique, which has been used to place constraints on the rate density of source populations, could use single detections from the shot noise component to interrogate the temporal dimension of the GW background signal (Howell et al. 2007a,b; Coward 2008; Howell et al. 2010).

Although the AGB signals discussed here remain speculative, and the estimated rates are still highly uncertain, detection of the GW emission mechanisms associated with SL-GRB events could yield important payoffs. This could be possible should locally observed SL-GRBs produce the necessary triggers for multi-messenger observations. Coupled with a single-source detection, an AGB signal could provide constraints on the high-z evolution of the highly flux-limited SL-GRB population and would be a valuable probe of source rate and metallicity evolution.

ACKNOWLEDGMENTS

We gratefully thank P. Mészáros for agreeing to provide us with data for the model in Corsi & Mészáros (2009a) of the secular bar-mode instability. We also thank Christian Ott for a careful reading an early initial manuscript and for providing us with important feedback on post-collapse instabilities in core-collapse supernovae. The authors also gratefully acknowledge Vuk Mandic who carefully read the manuscript and made some insightful suggestions as part of the LIGO Scientific Collaboration review. LIGO was constructed by

the California Institute of Technology and Massachusetts Institute of Technology with funding from the National Science Foundation. This paper has LIGO Document Number LIGO-P100083.

REFERENCES

Abbott B. P. et al., 2008, Phys. Rev. D, 77, 2004
Abbott B. P. et al., 2010a, ApJ, 715, 1438
Abbott B. P. et al., 2010b, ApJ, 715, 1453
Allen B., Romano J., 1999, Phys. Rev. D, 59, 102001
Allen B. et al., 2002, Phys. Rev. D, 65, 122002
Andersson N. et al., 2009, preprint (astro-ph:0912.0384)
Arnett W. D., Bowers R. L., 1976, Microscopic Interpretation of Neutron Star Structure. Sep. Print Tex. Univ., Austin, USA, Center Partido Theory, ORO-3992-257, 53p
Baiotti L. et al., 2007, Phys. Rev. D, 75, 044023
Blair D., Ju L., 1996, MNRAS, 283, 648
Bloom J. S. et al., 2009, preprint (astro-ph:0902.1527)
Bonazzola S., Gourgoulhon E., 1996, A&A, 312, 675
Brown D., 2000, Phys. Rev. D, 62, 084024
Bucciantini N. et al., 2007, MNRAS, 368, 1717
Bucciantini N. et al., 2009, MNRAS, 396, 2038
Butler N. R., Bloom J. S., Poznanski D., 2010, ApJ, 711, 495
Centrella J. M. et al., 2001, ApJ, 550, L193
Chandrasekhar S., 1969, Ellipsoidal Figures of Equilibrium. Yale University Press, New Haven
Chandrasekhar S., 1970, Phys. Rev. Lett., 24, 611
Chapman R. et al., 2007, MNRAS, 382, L21
Cobb B. E. et al., 2006, ApJ, 645, L113
Corsi A., Mészáros P., 2009a, ApJ, 702, 1171
Corsi A., Mészáros P., 2009b, Class. Quant. Grav., 26, 204016
Coward D. M., 2005, MNRAS, 360, L77
Coward D. M., 2008, MNRAS, 389, L43
Coward D. M., Burman R. R., 2005, MNRAS, 361, 362
Coward D. M., Burman R. R., Blair D. G., 2001, MNRAS, 324, 1015
Coward D., Regimbau T., 2006, New Astron. Rev., 50, 461
Cutler C., 2002, Phys. Rev. D, 66, 084025
Dai Z. G., Lu T., 1998, A&A, 333, L87
Dalal N., Holz D. E., Hughes S. A., B J., 2006, Phys. Rev. D, 74
Dall Osso S., Stella L., 2007, Ap&SS, 308, 119
DallOsso S. et al., 2009, MNRAS, 398, 1869
DallOsso S., Stratta G., Guetta D., Covino S., De Cesare G., Stella L., 2010, preprint (astro-ph:1004.2788)
Dimmelmeier H. et al., 2008, Phys. Rev. D, 78
Drasco S., Flanagan E. E., 2003, Phys. Rev. D, 67, 8
Duncan R. C., Thompson C., 1992, ApJ, 392, L9
Evans P. A. et al., 2009, MNRAS, 397, 1177
Fan Y.-H., Xu D., 2006, MNRAS, 372, L19
Faucher-Giguère C.-A., Kaspi V. M., 2006, ApJ, 643, 332
Feng L., Fox D. B., 2010, MNRAS, 404, 1018
Ferrari V., Matarrese S., Schneider R., 1999a, MNRAS, 303, 247
Ferrari V., Matarrese S., Schneider R., 1999b, MNRAS, 303, 258
Fotopoulos N. V., 2008, J. Phys. Conf. Ser., 122, 012032
Friedman J., Schutz B., 1978, ApJ, 222, 281
Grishchuk L., 1975, Sov. Phys. JETP, 40, 409
Guetta D., Della Valle M., 2007, ApJ, 657, L73
Hartmann D. H., 2010, Nat Phys., 6, 241
Hild S., Chelkowski S., Freise A., 2008, preprint (gr-qc:0810.0604)
Hild S. et al., 2010, Class. Quant. Grav., 27, 015003
Hopkins A. M., Beacom J. F., 2006, ApJ, 651, 142
Horowitz C. J., 2010, preprint (astro-ph:1008.0402)
Howell E. et al., 2004, MNRAS, 351, 1237
Howell E. et al., 2007a, MNRAS, 377, 719
Howell E. et al., 2007b, ApJ, 666, L65
Howell E. et al., 2010, in Hartnett J. G., Abbott P. C., eds, Proc. of the Frontiers of Fundamental and Computational Physics: 10th Int. Symp. Vol., 1246. AIP, New York, p. 203
Imerito A. et al., 2008, MNRAS, 391, 405
Janka H. T. et al., 2007, Phys. Rep., 442, 38
Kaminder A. D. et al., 2007, A&SS, 308, 423
Kobayashi S., Mészáros P., 2003, ApJ, 589, 861
Kocevski D., West A. A., Modjaz M., 2009, ApJ, 702, 377
Kochanek C. S., Piran T., 1993, ApJ, 417, L17
Konno K., Obata T., Kojima Y., 2000, A&A, 356, 234
Kouveliotou C. et al., 1993, ApJ, 413, L101
Lai D., Shapiro S. L., 1995, ApJ, 442, 259
Langer N., Norman C. A., 2006, ApJ, 638, L63
Li L., 2008, MNRAS, 388, 1487
Liang E. et al., 2007a, ApJ, 662, 1111
Liang E., Zhang B., Zhang B., 2007b, ApJ, 670, 565
Lin L.-M., 2007, Phys. Rev. D., 76, 081502
LSC VIRGO Collaboration, 2009, Nat, 460, 990
Lyons N. et al., 2010, MNRAS, 402, 705
MacFadyen A. I., Woosley S. E., Heger A., 2001, ApJ, 550, 410
Maggiore M., 2000, Phys. Rep., 331, 6
Mazzali P. A. et al., 2006, Nat, 442, 1018
Mendell G., 2001, Phys. Rev. D, 64, 044009
Mészáros P., Rees M. J., 1992, MNRAS, 257, 29
Metzger B. D. et al., 2007, ApJ, 659, 561
Modjaz M. et al., 2008, ApJ, 135, 1136
Murase K. et al., 2006, ApJ, 651, L5
Nakar E., 2007, Phys. Rept., 442, 166
New K. C. B., Centrella J. M., Tohline J. E., 2000, Phys. Rev. D, 62, 064019
Nousek J. A. et al., 2006, ApJ, 642, 389
Ostriker J. P., Gunn J. E., 1969, ApJ, 157, 1395
Ott C. D., 2009, Class. Quant. Grav., 26, 063001
Ott C. D., Ou S., Tohline J. E., Burrows A., 2005, ApJ, 625, L119
Ou S.-L., Tohline J. E., Lindblom L., 2004, ApJ, 617, 490
Owen B. J., 2005, Phys. Rev. Lett., 95, 211101
Owen B. J., Lindblom L., Cutler C., Schutz B. F., Vecchio A., Andersson N., 1998, Phys. Rev. D, 58, 084020
Palomba C., 2000, A&A, 354, 163
Palomba C., 2001, A&A, 367, 525
Panaitescu, 2008, MNRAS, 383, 1143
Peebles P. J. E., 1993, Principles of Physical Cosmology, 1st edn. Princeton Univ. Press, Princeton NJ
Pian E. et al., 2006, Nat, 442, 1011
Porciani C., Madau P., 2000, ApJ, 548, 522
Rao S. M., Turnshek D. A., Nestor D. B., 2006, ApJ, 636, 610
Regimbau T., 2007, Phys. Rev. D, 75, 043002
Regimbau T., de Freitas Pacheco J., 2000, A&A, 359, 242
Regimbau T., de Freitas Pacheco J., 2006a, A&A, 447, 1
Regimbau T., de Freitas Pacheco J., 2006b, ApJ, 642, 455
Regimbau T., Hughes S. A., 2009, Phys. Rev. D, 79, 062002
Regimbau T., Mandic V., 2008, Classical Quant. Gravity, 25, 184018
Rezzolla L., Lamb F. K., Marković D., Shapiro S. L., 2001, Phys. Rev. D, 64, 104013
Ruderman M., 1972, ARA&A, 10, 427
Saijo M. et al., 2001, ApJ, 548, 919
Salvaterra R., Chincarini G., 2007, ApJ, 656, L49
Sari R., Narayan R., Piran T., 1998, ApJ, 497, L17
Scheidegger S. et al., 2008, A&A, 490, 231
Scheidegger S. et al., 2010, A&A, accepted (astro-ph:1001.1570)
Shibata M., Karino S., 2004, Phys. Rev. D, 70, 4022
Shibata M., Baumgarte W., Shapiro S., 2000, ApJ, 542, 453
Shibata M., Karino S., Eriguchi Y., 2002, MNRAS, 334, L27
Shoemaker D., 2001, Future Limits to Sensitivity, http://www.ligo.caltech.edu/docs/G/G010026-00.pdf
Soderberg A. M. et al., 2006a, Nat, 422, 1014
Soderberg A. M., Nakar E., Berger E., Kulkarni S. R., 2006b, ApJ, 638, 930
Soria R., Perna R., Pooley D., Stella L., 2008, preprint (astro-ph:0811.3605)
Stamatikos M., Gehrels N., Halzen F., Mészáros P., Roming P. W. A., 2009, Contributed to The Astro2010 Decadal Survey, Committee for a Decadal Survey of Astronomy and Astrophysics. Nat. Res. Council, Nat. Acad. Press, preprint (astro-ph:0902.3022)

Stella L. et al., 2005, ApJ, 634, L165
Tanvir N. R. et al., 2009, Nat, 461, 1254
Thompson C., Duncan R. C., 1993, ApJ, 408, 194
Thompson C., Chang P., Quataert E., 2004, ApJ, 611, 380
Toma K. et al., 2007, ApJ, 659, 1420
Usov V. V., 1992, Nat, 357, 472
Vink J., Kuiper L., 2006, MNRAS, 370, L14
Vink J. S., de Koter A., 2005, A&A, 442, 587
Virgilii F. J., Liang E.-W., Zhang B., 2008, MNRAS, 392, 91
Virgili F. J., Liang E., Zhang B., 2009, MNRAS, 392, 91
Woosley S. E., 1993, ApJ, 405, 273
Woosley S., Janka T., 2005, Nat. Phys., 1, 147
Woosley S. E., Bloom J. S., 2006, ARA&A, 44, 507
Woosley S. E., Heger A., 2006, ApJ, 637, 914
Yamazaki R., 2009, ApJ, 690, L118
Yoon S. C., Langer N., 2005, A&A, 443, 643
Yu Y. W., Liu X. W., Dai Z. G., 2007, ApJ, 671, 637
Yu Y., Cheng K. S., Cao X., 2010, ApJ, 715, 477
Zhang B., Mèszàros P., 2001, ApJ, 552, L35
Zhang D., Dai Z. G., 2009, ApJ, 718, 841
Zhang B. et al., 2006, ApJ, 642, 354

APPENDIX A: THE EFFECT OF COSMIC METALLICITY ON A GW BACKGROUND SIGNAL

To illustrate the effect of metallicity dependence on calculations of a GW background signal, in Fig. A1 we reproduce the curves of Figs 6 and 8 for the rate $r_{\rm P}$. We add thick lines showing a metallicity-independent ($\epsilon = 1.0$) source rate evolution. We see that including a metallicity cut-off of $\epsilon = 0.1$ gives a higher signal at lower frequencies. This is a result of the greater contribution from high-z sources illustrated in Fig. 2. As indicated by the results in Tables 3–6, this effect increases the S/N estimates.

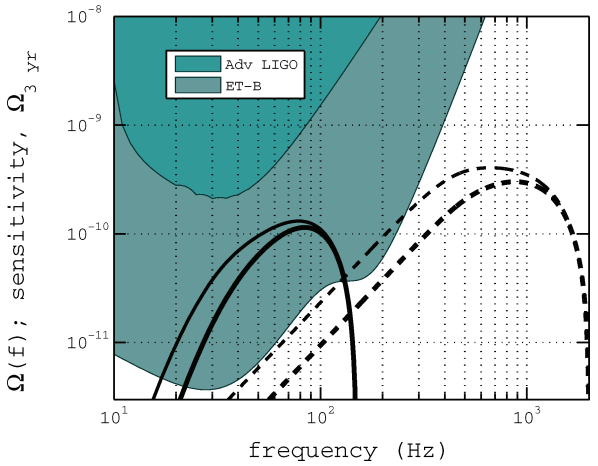

Figure A1. To illustrate the effect of metallicity dependence on the GW background signal we reproduce the curves of Figs 6 and 8 for rate $r_{\rm P}$. We add thick lines showing a metallicity-independent source rate evolution assuming $\epsilon = 1.0$. We see that including metallicity dependence shifts the background spectrum slightly to lower frequency.

This paper has been typeset from a TEX/LATEX file prepared by the author.